

## Fe-Doping Effect on the Bi<sub>3</sub>Ni Superconductor Microstructure

Silvio Henrique Gonsalves<sup>a</sup>, João Frederico Haas Leandro Monteiro<sup>a</sup>, Adriane Consuelo

Da Silva Leal<sup>a</sup>, André Vitor Chaves de Andrade<sup>a</sup>, Gelson Biscaia de Souza<sup>a</sup>, Ezequiel Costa Siqueira<sup>a</sup>,

Francisco Carlos Serbena<sup>a</sup>, Alcione Roberto Jurelo<sup>a\*</sup>

<sup>a</sup> Departamento de Física, Universidade Estadual de Ponta Grossa - UEPG, Av. Gen. Carlos Cavalcanti, 4748, 84.030-000, Ponta Grossa, PR, Brazil

Received: July 15, 2016; Revised: January 19, 2017; Accepted: February 18, 2017

The substitution effects of Fe ion on the structure of the intermetallic Bi<sub>3</sub>Ni<sub>1-x</sub>Fe<sub>x</sub> (0 ≤ x ≤ 0.10) superconductor were studied. The morphology of samples consists of an inhomogeneous laminar slab-like microstructure. The main phase corresponds to Bi<sub>3</sub>Ni<sub>1-x</sub>Fe<sub>x</sub> with an orthorhombic structure (*Pnma*), but with very small quantities of impurities of BiNi and Bi as revealed by X-ray diffraction. SEM and AFM reveal that the Bi<sub>3</sub>Ni<sub>1-x</sub>Fe<sub>x</sub> phase consists of two regions. One region is Bi richer and Ni and Fe poorer than the other region. Raman spectroscopy revealed two phonon modes at room temperature. No significant changes were observed in the spectra with Fe doping and in different regions of the Bi<sub>3</sub>Ni<sub>1-x</sub>Fe<sub>x</sub> phase. Superconductivity is observed below a transition temperature  $T_C = 4$  K and regardless of iron doping.

**Keywords:** Bi<sub>3</sub>Ni, Superconductor, Intermetallic alloys, Iron

### 1. Introduction

The coexistence of superconductivity and magnetism is a phenomenon of great interest in condensed matter physics. In almost all materials, these two fundamental states are highly competitive and destroy the superconductivity. Compounds based in Bi-Ni, such as LaO<sub>1-δ</sub>NiBi<sup>1</sup>, CeNiBi<sub>2</sub><sup>2</sup> and Bi<sub>3</sub>Ni<sup>3</sup>, present this complex phenomenon. In the superconductor Bi<sub>3</sub>Ni compound, with critical temperature  $T_C$  around 4.1 K<sup>3</sup>, the coexistence of superconductivity and ferromagnetism is observed, with superconductivity emerging in the ferromagnetically ordered phase<sup>4</sup>.

The stoichiometric Bi<sub>3</sub>Ni is described as an intermetallic alloy with an orthorhombic crystallographic structure of CaLiSi<sub>2</sub>-type, 16 atoms per unit cell and space group *Pnma*<sup>5</sup>. Ruck *et al.* studied the crystal structure of Bi<sub>3</sub>Ni using quantum chemical calculations. According to their results, the Ni atoms have a capped trigonal prismatic coordination of Bi atoms with strong bonds Ni-Bi and Ni-Ni<sup>6</sup>. Besides the Ni-Bi phase diagram, others phase diagrams such as Rh-Bi<sup>7-8</sup> and Co-Bi<sup>9</sup> have been explored to search for new superconductors. For RhBi<sub>4</sub> and Rh<sub>3</sub>Bi<sub>14</sub><sup>5</sup>, superconductivity was observed at a critical temperature  $T_C$  of 2.8 K and 3.2 K, respectively. For the CoBi<sub>3</sub> compound, synthesized using a high-pressure and high-temperature technique,  $T_C$  is around 0.5 K.

Although the Bi<sub>3</sub>Ni compound is known as a superconductor since 1948<sup>3</sup>, there were few reports about this material. Pineiro *et al.* studied the possible coexistence of superconductivity and magnetism in Bi<sub>3</sub>Ni and showed that it presents a

ferromagnetic characteristic up to 750 K, well above the Ni Curie temperature<sup>10</sup>. Herrmannsdorfer *et al.* demonstrated the coexistence of ferromagnetic and superconducting states in Bi<sub>3</sub>Ni nanostructures. Superconductivity confined in Bi<sub>3</sub>Ni emerges in the ferromagnetically ordered phase and is stable up to high magnetic fields<sup>4</sup>. Zhu *et al.* investigated anisotropy in superconducting and normal state properties of Bi<sub>3</sub>Ni single crystals<sup>11</sup>. They demonstrated from electron spin resonance that ferromagnetic fluctuations exist on the surface of the crystal below 150 K.

In this study, we describe the substitution effects of Fe ion in the structure of the Bi<sub>3</sub>Ni<sub>1-x</sub>Fe<sub>x</sub> (x = 0.00, 0.05 and 0.10) superconductor. The samples were prepared by the solid-state reaction method and characterized by X-ray diffraction, optical and scanning electron microscopy with energy dispersive spectroscopy, atomic force microscopy and Raman spectroscopy. It was observed that the main phase corresponds to Bi<sub>3</sub>Ni<sub>1-x</sub>Fe<sub>x</sub>, but with small quantities of BiNi and Bi as impurities. From SEM and AFM, two regions were observed in all samples: white and gray. The white region is richer in Bi and poorer in Ni and Fe than the gray region. Observations from atomic force microscopy experiments, in magnetic mode, showed the presence of magnetic interactions in the range of 500 nm. Raman spectra were obtained and two phonon modes were observed, with no peak shift dependence with Fe doping.

### 2. Experimental Details

Polycrystalline samples of Bi<sub>3</sub>Ni<sub>1-x</sub>Fe<sub>x</sub> (0 ≤ x ≤ 0.10) were prepared by the solid-state reaction method using Bi

\* e-mail: arjurelo@uepg.br

pieces and Ni and Fe powders. Appropriate amounts were mixed with help of a pestle and mortar for around one hour. Then, the product was pelletized and encapsulated in an evacuated quartz tube for melting. Samples were heated at 1000 °C for 24 h and slowly cooled to room temperature. The characterization was performed by X-ray diffraction (XRD), optical and scanning electron microscopy (SEM) with energy dispersive spectroscopy (EDS), atomic force microscopy (AFM) and Raman spectroscopy. XRD experiments were carried out using a Rigaku diffractometer with  $\text{CuK}\alpha$  radiation and XRD patterns were collected from 5° to 120° in the  $2\theta$  range with 0.006 step and 6 s counting time. The unit cell parameters were refined by the Rietveld-Le Bail method using the GSAS+ExpGui software<sup>12-13</sup>. Samples were also characterized in air and at room temperature using a commercial AFM system (SPM-9600 Shimadzu) in non-contact and magnetic modes. The images were processed to remove the low-frequency noise. The images were obtained with silicon cantilever with a magnetized cobalt coating (MFMR-10 from Nano World Innovative Technologies). The probe was Al-coated on the detector side. The cantilevers had a resonant frequency of approximately 75 kHz, with nominal spring constant of 2.8 N/m. Unpolarized confocal Raman measurements were performed with a Bruker Senterra R200-532 spectrometer equipped with an Olympus optical microscope and with a thermo-electrically cooled CCD detector equipped with a solid state laser with  $\lambda = 532$  nm. A 50X objective microscopic lens was used at different regions of the samples. A circular pin-hole of 50  $\mu\text{m}$  was used with an estimated spot size of 2  $\mu\text{m}$  at sample surface. Acquisition times were around 20 s with an incident laser power density below  $60 \times 10^4 \text{ W/cm}^2$  in order to avoid sample heating. The magnetic properties were measured by using a physical property measurement system (PPMS, Quantum Design) and a vibrating sample measurement system (VSM). DC magnetization measurements were performed as a function of temperature under zero-field-cooling (ZFC) and field-cooling (FC) conditions.

### 3. Results and Discussion

The X-ray powder diffraction patterns at room temperature of polycrystalline  $\text{Bi}_3\text{Ni}_{1-x}\text{Fe}_x$  samples with  $x = 0.00$ ,  $x = 0.05$  and  $x = 0.10$  are displayed in Figure 1. It was observed that the main phase corresponds to  $\text{Bi}_3\text{Ni}_{1-x}\text{Fe}_x$  with orthorhombic structure ( $Pnma$ ) and with small quantities of impurities of BiNi and Bi. No Ni as impurity was detected. The unit cell parameters, atomic factor parameters and agreement factors obtained by Rietveld-Le Bail method are summarized in Table 1. Specifically for  $\text{Bi}_3\text{Ni}_{1-x}\text{Fe}_x$  samples, the behavior of lattice parameters as a function of iron doping can be seen in Table 1. The value of the lattice parameter  $a$  is approximately constant with 8.8832 (1) Å for  $x = 0.00$  and 8.8837 (1) Å for  $x = 0.10$ . On the other hand,  $b$  and  $c$  increase with iron

doping. The  $b$  parameter increased from 4.0997 (1) Å for  $x = 0.00$  to 4.10283 (9) Å for  $x = 0.10$  while the  $c$  parameter increased from 11.4839 (2) Å to 11.4876 (1) Å. Also, the unit cell volume increases from 418.23 (1) Å<sup>3</sup> for  $x = 0.00$  to 418.71 (1) Å<sup>3</sup> for  $x = 0.10$ . The lattice parameters and unit cell volume for pure  $\text{Bi}_3\text{Ni}$  ( $x = 0.00$ ) derived from least squares refinement are in agreement with the published result obtained in another study<sup>14</sup>. Also, from Table 1, we can observe that  $R_{wp}$  ( $R$  – weighted pattern) and  $\chi^2 = \sqrt{R_{wp}/R_e}$  (goodness-of-fit) are small and therefore reliable.

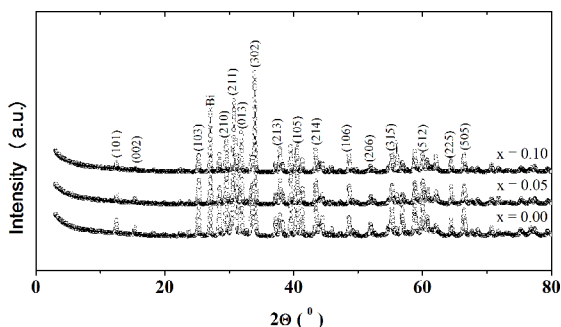


**Figure 1.** XRD patterns taken at room temperature of polycrystalline  $\text{Bi}_3\text{Ni}_{1-x}\text{Fe}_x$  sample.

**Table 1.** Lattice parameters  $a$ ,  $b$ ,  $c$  and unit cell volume  $V$  for polycrystalline  $\text{Bi}_3\text{Ni}_{1-x}\text{Fe}_x$  samples. Numbers in parentheses indicate the standard deviation.

| $\text{Bi}_3\text{Ni}$ ( $x = 0.00$ )                        |                     |                          |
|--|---------------------|--------------------------|
| Phases   | Cell parameters (Å) | Volume (Å <sup>3</sup> ) |
| $\text{Bi}_3\text{Ni}$                                       | $a = 8.8832$ (1)    | 418.23 (1)               |
|  | $b = 4.0997$ (1)    |                          |
|  | $c = 11.4839$ (2)   |                          |
| $*R_{wp} = 7.52$ % and $\chi^2 = 2.315$                      |                     |                          |
| $\text{Bi}_3\text{Ni}_{0.95}\text{Fe}_{0.05}$ ( $x = 0.05$ ) |                     |                          |
| Phases   | Cell parameters (Å) | Volume (Å <sup>3</sup> ) |
| $\text{Bi}_3\text{Ni}$                                       | $a = 8.8819$ (1)    | 418.18 (2)               |
|  | $b = 4.1002$ (1)    |                          |
|  | $c = 11.4830$ (2)   |                          |
| $*R_{wp} = 7.55$ % and $\chi^2 = 1.749$                      |                     |                          |
| $\text{Bi}_3\text{Ni}_{0.90}\text{Fe}_{0.10}$ ( $x = 0.10$ ) |                     |                          |
| Phases   | Cell parameters (Å) | Volume (Å <sup>3</sup> ) |
| $\text{Bi}_3\text{Ni}$                                       | $a = 8.8837$ (1)    | 418.71 (1)               |
|  | $b = 4.10283$ (9)   |                          |
|  | $c = 11.4876$ (1)   |                          |
| $*R_{wp} = 8.66$ % and $\chi^2 = 2.003$                      |                     |                          |

Figures 2(a) and 2(b) show the microstructure of the polycrystalline  $\text{Bi}_3\text{Ni}_{1.00}\text{Fe}_{0.00}$  sample as revealed by SEM using backscattered electrons. From panel (a), we can clearly observe a granular structure with several pores. It also shows that the sample is inhomogeneous at micrometric scale, with

white and gray regions. The same structure is observed for all samples. Their composition measured by EDS will be discussed later. Figure 2(b) shows in higher magnification several microcracks that are aligned approximately parallel to a horizontal direction in the photograph. The origin of these cracks may be due to thermal expansion anisotropy as observed in REBa<sub>2</sub>Cu<sub>3</sub>O<sub>7- $\delta$</sub>  (RE = rare earth)<sup>15</sup> or due to weak bonding between the laminar grains as observed in iron-based superconductors<sup>16</sup>.

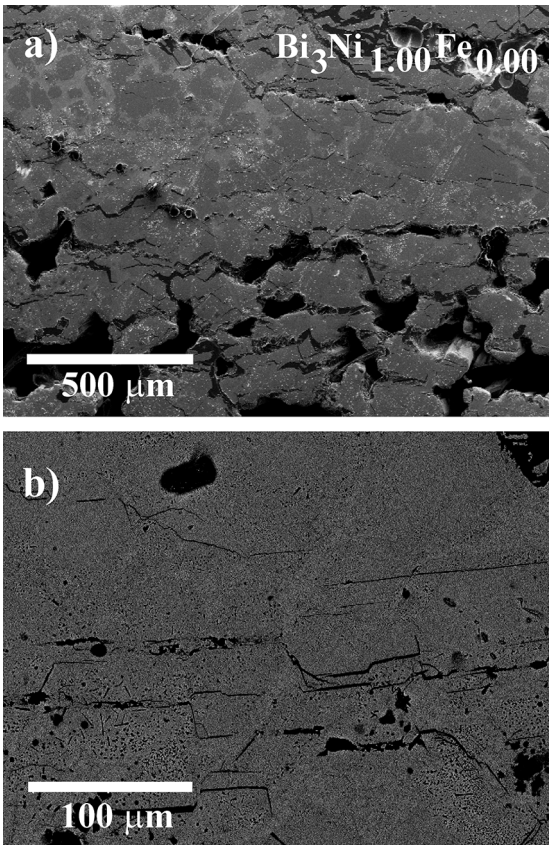


**Figure 2.** (a) Backscattered electrons SEM image of the polycrystalline of Bi<sub>3</sub>Ni<sub>1-x</sub>Fe<sub>x</sub> ( $x = 0.00$ ) sample. The stacked lamellar structure is shown in more detail in (b).

Figure 3 show the microstructure of polycrystalline samples of Bi<sub>3</sub>Ni<sub>1-x</sub>Fe<sub>x</sub> with (a)  $x = 0.00$  and (b)  $x = 0.10$  in more detail. Two regions, labeled white and gray, are clearly observed. If the same image of the polycrystalline sample with  $x = 0.00$  is observed by optical microscopy, two regions are also distinguished in the upper inset. In the lower inset, the surface morphology of the polycrystalline Bi<sub>3</sub>Ni<sub>0.90</sub>Fe<sub>0.10</sub> sample was analyzed with atomic force micrograph in phase mode using a Si probe and revealed also two regions, one darker on the right side and another white on the left side of the figure. We cannot distinguish each of these two regions corresponds to the two regions observed by SEM, but they maybe correlated.

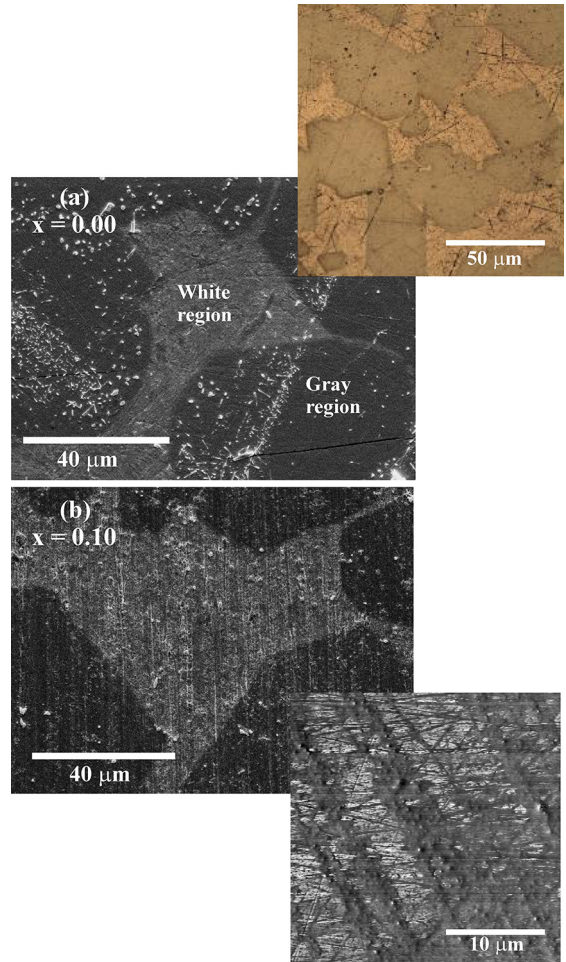


**Figure 3.** Backscattered electrons SEM micrographs for a polycrystalline sample of Bi<sub>3</sub>Ni<sub>1-x</sub>Fe<sub>x</sub> with (a)  $x = 0.00$  and (b)  $x = 0.10$ . We can clearly observe two regions, labeled white and gray. Upper inset: optical image of the polycrystalline of Bi<sub>3</sub>Ni sample. Lower inset: atomic force micrograph of a polycrystalline Bi<sub>3</sub>Ni<sub>0.90</sub>Fe<sub>0.10</sub> sample in phase mode using a Si probe.

If Figure 3(b) is magnified, several lamellae are observed in both white (Figure 4(a)) and gray (Fig. 4(b)) regions. Their thickness is around 500 nm and they are aligned across several grains. While in the white region the porosity appears to be low, in the gray regions, the porosity is higher. Also the pores appear to be aligned parallel to the lamellae in the gray region. It is possible to observe also in Figs. 3(b) and 4 that this microstructure runs across several white and gray regions, leaving the possibility our samples to be textured.

In view of the different regions observed from X-ray and SEM at different samples, we decided to analyze the chemical composition using energy dispersive spectroscopy (EDS). Local composition of the Bi<sub>3</sub>Ni and Bi<sub>3</sub>Ni<sub>0.90</sub>Fe<sub>0.10</sub> samples was determined by EDS in different positions on the sample surface and in using areas of  $4 \times 4 \mu\text{m}^2$ . Table 2 shows the compositions measured in different regions. The results

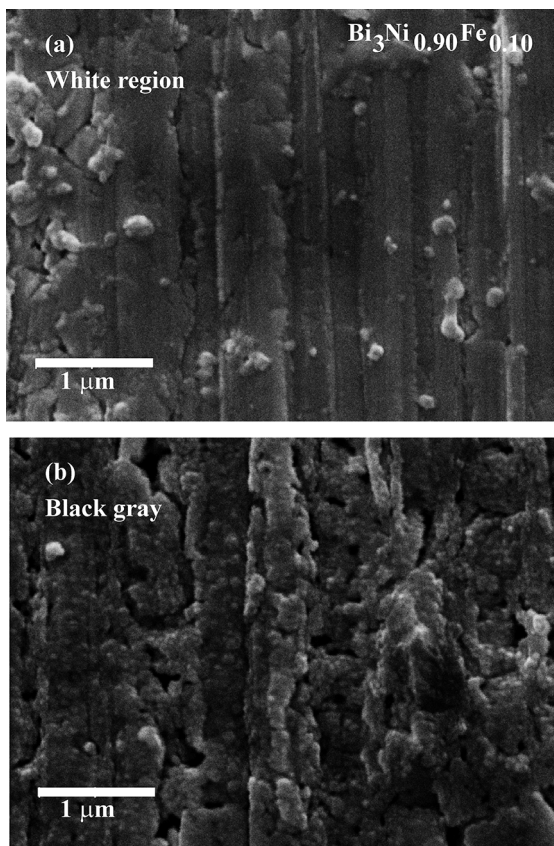


**Figure 4.** SEM micrograph of polycrystalline sample of  $\text{Bi}_3\text{Ni}_{0.90}\text{Fe}_{0.10}$  for (a) white and (b) gray regions.

showed that there is variation in the chemical composition between the white and gray regions. This chemical composition difference is smaller in the  $\text{Bi}_3\text{Ni}$  than in the  $\text{Bi}_3\text{Ni}_{0.90}\text{Fe}_{0.10}$ . The white region is richer in Bi and poorer in Ni than the gray region for  $\text{Bi}_3\text{Ni}$  samples. When Fe is added, its solubility is higher in the gray region (14 %) than in the white region (8 %). Also, the ratio between Bi/Ni is constant (10) for the gray phase for the  $\text{Bi}_3\text{Ni}$  and  $\text{Bi}_3\text{Ni}_{0.90}\text{Fe}_{0.10}$  samples. For the white region, this ratio increases when Fe is added. The XRD experiment shown in Figs. 1(a-c) revealed that the white and gray regions have the same atomic structure, despite of the slight different chemical composition due to the different solubility of the elements revealed in the SEM.

Figure 5 show AFM images of  $10 \times 10 \mu\text{m}^2$  area for  $\text{Bi}_3\text{Ni}_{0.90}\text{Fe}_{0.10}$  sample. Both images were obtained under

ambient conditions in (a) phase mode and (b) topographic mode using a magnetized Co-coated probe for the same region. In the upper inset, image (a) is shown in more detail. While Figs. 5(a) and 5(b) show different regions in respect of the interaction between the AFM probe and the sample surface with no clear observed pattern, in the inset of Fig. 5(b) it is observed several magnetic fringes with a width of approximately 500 nm. These results may show that our sample is magnetically inhomogeneous. The structure was observed in all samples with Fe concentration equals to  $x = 0.00$ ,  $x = 0.05$  and  $x = 0.10$ . The  $x = 0.00$  and  $x = 0.10$  samples were rotated  $90^\circ$  degrees and the observed magnetic fringe pattern did not change orientation with the sample. We do not think that this observed magnetic fringe pattern is related with the lamellae structure observed in Figs. 4 since this pattern was also observed in samples with  $x = 0.00$  (Fig. 4(a)).

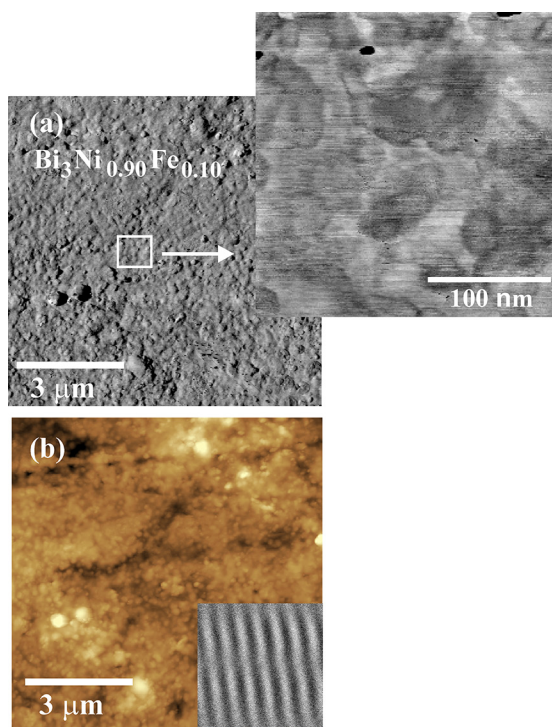


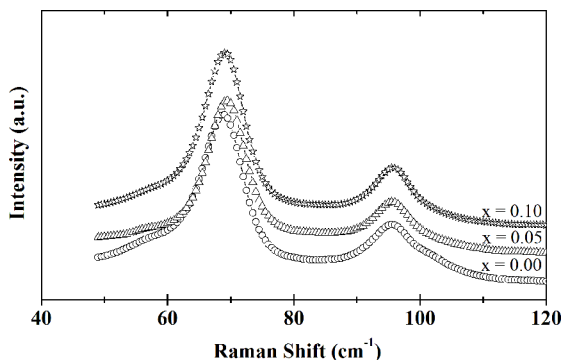
**Figure 5.** Atomic force micrographs of a polycrystalline  $\text{Bi}_3\text{Ni}_{0.90}\text{Fe}_{0.10}$  sample in the same region in (a) phase mode and (b) topographic mode using a magnetized Co-coated Si probe. Upper inset: The image (a) in higher magnification. Lower inset: The same region of (b) was observed in magnetic mode.

**Table 2.** Local composition of the  $\text{Bi}_3\text{Ni}$  and  $\text{Bi}_3\text{Ni}_{0.90}\text{Fe}_{0.10}$  samples, as determined by EDS in different positions on the sample surface. The EDS analyses were performed in areas of  $4 \times 4 \mu\text{m}^2$ .

| Samples                                       | Composition (wt.%) |        |        |        |        |        |
|---|--------------------|--------|--------|--------|--------|--------|
|   | Region             |        |        |        |        |        |
|   | White              |        |        | Gray   |        |        |
|   | Bi (%)             | Ni (%) | Fe (%) | Bi (%) | Ni (%) | Fe (%) |
| $\text{Bi}_3\text{Ni}_{1.00}\text{Fe}_{0.00}$ | 95.2               | 4.7    | 0.0    | 91.0   | 9.0    | 0.0    |
| $\text{Bi}_3\text{Ni}_{0.90}\text{Fe}_{0.10}$ | 90.5               | 1.6    | 7.9    | 78.0   | 7.8    | 14.2   |

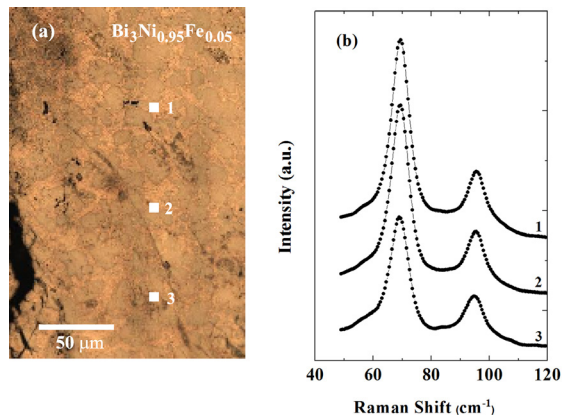
Raman spectroscopy is a powerful tool to detect changes at the microscopic level. Then, the search for specific features in the Raman spectra could shed new light in the effect of iron substitution in Bi<sub>3</sub>Ni<sub>1-x</sub>Fe<sub>x</sub> samples. We probed the samples with different power densities, from 6 to 60 x 10<sup>4</sup> W/cm<sup>2</sup> (applied power from 2 to 20 mW) at room temperature in order to investigate possible suppression or enlargement of active Raman modes as a function of the laser power density. Different locations on the sample surface were probed in order to assure spectra representability.

Figure 6 shows Raman spectra of Bi<sub>3</sub>Ni<sub>1-x</sub>Fe<sub>x</sub> samples with  $x = 0.00$ ,  $x = 0.05$  and  $x = 0.10$  obtained at room temperature with an applied power of 10 mW (30 x 10<sup>4</sup> W/cm<sup>2</sup>). This power had the best signal-to-noise ratio with well resolved Raman peaks. The Raman spectra showed 2 Raman modes at  $69 \pm 1$  and  $96 \pm 1$  cm<sup>-1</sup>. The line observed in 69 cm<sup>-1</sup> is the most prominent, while a weaker band is observed at 96 cm<sup>-1</sup>. The phonon modes observed in this study show typical Lorentzian line shapes without asymmetry. The two peaks were not identified with any specific displacement mode and to the best of our knowledge, there is no mode identification for this material in the literature. No significant changes were observed in the spectra with Fe doping.



**Figure 6.** Room temperature Raman spectra of polycrystalline Bi<sub>3</sub>Ni<sub>1-x</sub>Fe<sub>x</sub> samples.

To study the effect of sample inhomogeneity in the Raman spectra modes, we sampled the polycrystalline Bi<sub>3</sub>Ni<sub>0.95</sub>Fe<sub>0.05</sub>, with measurements performed at different locations across the sample 50 μm apart. A power of 10 mW was used. The positions taken for the spectra are displayed in Fig. 7(a) and the corresponding Raman spectra are shown in figure 7(b). The peak positions of the spectra do not change with the location on the sample, despite the presence of the inhomogeneities (white and gray regions, apart from BiNi and Bi impurities) present in the samples. On the other hand, the intensity of the peaks varied with the position. Therefore, it can be concluded that the presence of small inhomogeneities does not shift the Raman peaks but change their intensities.



**Figure 7.** (a) Mapping of Bi<sub>3</sub>Ni<sub>0.95</sub>Fe<sub>0.05</sub> sample for a laser power of 10 mW. Measurements were performed in 3 steps spaced by 50 μm starting from the top (1) and (b) the corresponding Raman spectra measured at room temperature.

Magnetization as a function of temperature of Bi<sub>3</sub>Ni<sub>1-x</sub>Fe<sub>x</sub> samples with  $x = 0.00$ ,  $x = 0.05$  and  $x = 0.10$  is shown in Figure 8. Figure depicts the DC magnetic susceptibility in zero-field-cooled (ZFC) situation in the temperature range 3-5 K and at an applied field  $H = 10$  Oe. Superconductivity is observed below a transition temperature  $T_C = 4$  K and regardless of iron doping. This is an important aspect of this study and more detailed investigations of the iron doping effects on the intermetallic Bi<sub>3</sub>Ni<sub>1-x</sub>Fe<sub>x</sub> ( $0 \leq x \leq 0.10$ ) superconductor is needed. One important aspect is the coexistence of superconductivity and magnetism for low concentrations of iron<sup>17</sup>.

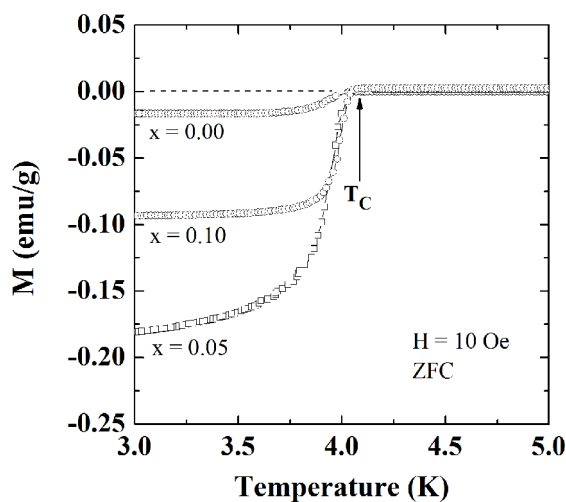


**Figure 8.** Magnetization as a function of temperature in ZFC situation at  $H = 10$  Oe for samples with  $x = 0.00$ ,  $x = 0.05$  and  $x = 0.10$ .

From the phase diagram of Bi-Fe, Bi<sub>3</sub>Fe samples may not be formed<sup>18</sup>. In this study, we did not observe any difference in the XRD diffractograms in samples with different Fe

concentrations. SEM showed only small differences in stoichiometry of the  $\text{Bi}_3\text{Ni}_{1-x}\text{Fe}_x$  phase for all Fe concentrations. Also, the Raman spectra were the same for samples with different Fe concentrations, even for the white and gray regions. Therefore, we conclude that Fe completely substitute Ni for all concentrations studied (up to  $x = 0.10$ ).

## 4. Conclusions

Polycrystalline  $\text{Bi}_3\text{Ni}_{1-x}\text{Fe}_x$  ( $0 \leq x \leq 0.10$ ) superconductor was synthesized by the solid-state reaction method. Samples' morphology consisted of laminar slab-like crystals. From XRD, it was observed that the main phase corresponds to  $\text{Bi}_3\text{Ni}_{1-x}\text{Fe}_x$  with small quantities of BiNi and Bi as impurities. From SEM observations, two regions were observed. One region is richer in Bi and poorer in Ni and Fe than the other. Raman spectra were obtained and two phonon modes were observed, with no peak shift dependence with Fe doping. It was also observed that  $\text{Bi}_3\text{Ni}_{1-x}\text{Fe}_x$  show superconductivity below a transition temperature  $T_c = 4$  K.

## 5. Acknowledgements

This work was partially financed by CNPq under contract nº 472.746/2013-8.

## 6. References

- Kozhevnikov VL, Leonidova ON, Ivanovskii AL, Shein IR, Goshchitskii BN, Kar'kin AE. New superconductor with a layered crystal structure: Nickel oxybismuthide  $\text{LaO}_{1+x}\text{NiBi}$ . *JETP Letters*. 2008;87(11):649-651. DOI: 10.1134/S002136400811012X.
- Jung MH, Lacerda AH, Takabatake T. Magnetic and transport properties of the antiferromagnetic Kondo-lattice compound  $\text{CeNiBi}_2$ . *Physical Review B*. 2002;65(13):132405-132410. DOI: 10.1103/PhysRevB.65.132405.
- Alekseevskii N. Superconductivity of bismuth compounds. *Journal of Experimental and Theoretical Physics*. 1948;18:101-102.
- Herrmannsdörfer T, Skrotzki R, Wosnitzer J, Kohler D, Boldt R, Ruck M. Structure-induced coexistence of ferromagnetic and superconducting states of single-phase  $\text{Bi}_3\text{Ni}$  seen via magnetization and resistance measurements. *Physical Review B*. 2011;83(14):140501-140504. DOI: 10.1103/PhysRevB.83.140501.
- Fjellvåg H, Furuseth S. Structural properties of  $\text{Ni}_{1-x}\text{RhBi}_3$ . *Journal of the Less Common Metals*. 1987;128:177-183. DOI: 10.1016/0022-5088(87)90204-9.
- Ruck M, Söhnel T. Transmission-Optimized Single-Crystal Structure Determination and Electronic Structure of  $\text{Bi}_3\text{Ni}$ . *Zeitschrift für Naturforschung B*. 2006;61(7):785-791. DOI: 10.1002/Chin.200641005.
- Fujimori Y, Kan S, Shinozaki B, Kawaguti T. Superconducting and normal state properties of  $\text{NiBi}_3$ . *Journal of the Physical Society of Japan*. 2000;69(9):3017-3026. DOI: 10.1143/JPSJ.69.3017.
- Weitzer F, Schnelle W, Gil RC, Hoffmann S, Giedigkeit R, Grin Y. Phase-relationship and superconductivity in the Bi-rich part of the binary system Rh-Bi. *Calphad*. 2009;33(1):27-30. DOI: 10.1016/j.calphad.2008.07.016.
- Tencé S, Janson O, Krellner C, Rossner H, Schwarz U, Grin Y, et al.  $\text{CoBi}_3$ —the first binary compound of cobalt with bismuth: high-pressure synthesis and superconductivity. *Journal of Physics: Condensed Matter*. 2014;26(39):395701. DOI: 10.1088/0953-8984/26/39/395701.
- Martinez Piñeiro EL, Ruiz Herrera BL, Escudero R, Bucio L. Possible coexistence of superconductivity and magnetism in intermetallic  $\text{NiBi}_3$ . *Solid State Communications*. 2011;151(6):425-429. DOI: 10.1016/j.ssc.2011.01.005.
- Zhu X, Lei H, Petrovic C, Zhang Y. Surface-induced magnetic fluctuations in a single crystal  $\text{NiBi}_3$  superconductor. *Physical Review B*. 2012;86(2):24527-24531. DOI: 10.1103/PhysRevB.86.024527.
- Larson AC, Von Dreele RB. *GSAS General Structure Analysis System*. Los Alamos: Los Alamos National Laboratory; 1994.
- Toby BH. EXPGUI, A graphical user interface for GSAS. *Journal of Applied Crystallography*. 2001;34:210-213.
- Kumar J, Kumar A, Vajpayee A, Gahtori B, Sharma D, Ahluwalia PK, et al. Physical property and electronic structure characterization of bulk superconducting  $\text{Bi}_3\text{Ni}$ . *Superconductor Science Technology*. 2011;24(8):85002-85009. DOI: 10.1088/0953-2048/24/8/085002.
- Foerster CE, Serbena FC, Jurelo AR, Ferreira TR, Júnior Rodrigues P, Chinellato AL. Mechanical properties of  $\text{REBa}_2\text{Cu}_3\text{O}_{7-\delta}$  superconductor with RE obtained from xenotime mineral. *IEEE Transactions on Applied Superconductivity*. 2011;21(2):52-59. DOI: 10.1109/TASC.2010.2099656.
- Dias FT, Pinheiro LBLG, Souza GB, Serbena FC, Silva SA, Jurelo AR, et al. Nanoscratch and indentation fracture toughness in superconductor Ba-Fe-As single crystals with lamellar structure. *Tribology International*. 2014;79:84-91. DOI: 10.1016/j.triboint.2014.05.026.
- Gonsalves SH, Opatá YA, Pinheiro LBLG, Leal ACS, Monteiro JFHL, Siqueira EC, et al. Superconductivity and magnetism in intermetallic  $\text{Bi}_3\text{Ni}_{1-x}\text{Fe}_x$  superconductor. *Solid State Communications*. 2016;242:6-10. DOI: 10.1016/j.ssc.2016.05.005.
- Yoshida H, Shima T, Takahashi T, Kaneko T, Suzuki T, Kimura HM, et al. Magnetic properties of NiBi. *Journal of Magnetism and Magnetic Materials*. 2002;239(1-3):5-7. DOI: 10.1016/S0304-8853(01)00511-X.